Athens Journal of Technology and Engineering - Volume 9, Issue 4, December 2022 – Pages 281-304

Numerical Estimation of a Mode III Fracture Mechanics Parameter for a Three-Dimensional V-Notch on a Steel Bold

By Miltiades C. Elliotis[*]

In this work a couple of three-dimensional problems in the domain of linear elastic Fracture Mechanics are examined. These are problems of solid bodies (they could be steel bolds or rivets) with a surface crack singularity (V-notch). They are reduced to Laplace equation problems by considering a Lamé potential. The boundary singularity is numerically treated as per the singular function boundary integral method (SFBIM), which in the literature is known as one of the so-called Trefftz methods. Thus, the general solution of the governing equation, in the vicinity of the surface crack, is expressed as an asymptotic expansion, the coefficients of which are approximated by polynomials. The remaining numerical steps are followed according to this method with which very fast convergence and very high accuracy are observed. In fact, the CPU time and the numerical error recorded with this numerical technique are significantly smaller than those achieved with the finite element method (FEM) which was also used to solve the same problems. The calculated value of Mode III Fracture Mechanics parameter (FMP) indicates that there is no danger of crack propagation. Thus, the extension of the method to this category of problems is considered as a novel application of this algorithm in Fracture Mechanics.

Keywords: *Mode III Fracture Mechanics parameter, crack singularity, governing equation, singular function boundary integral method, local solution, Lamé potential*

Introduction

Force formulation in linear elasticity problems is not an easy task. Our attempt to overcome difficulties encountered in this category of engineering problems is a great challenge when we have to tackle three-dimensional problems. Such problems are treated by professionals and researchers in the fields of engineering, such as the construction industry, mechanical engineering, car industry and aerospace engineering. Their number is continuously growing due to the needs for new complicated structures, such as construction trusses, geodesic domes and tensegrity structures, mechanisms (made of metal alloys) used in robotics and biomedical engineering, vehicles and aircrafts with sensitive and complicated mechanical connections and many others. Thus, most engineering problems in the domain of Solid Mechanics are three-dimensional problems which lead the designers and researchers to the implementation of approaches which exhaust the

[*]Scientific Collaborator, Department of Mathematics and Statistics, University of Cyprus, Cyprus.

https://doi.org/10.30958/ajte.9-4-2 doi=10.30958/ajte.9-4-2

limits of computational resources. Also, in trying to solve particular problems in the fields of theoretical or applied Mechanics, exhibiting specific boundary singularities, engineers have to overcome several obstacles. Such problems are the elliptic equation problems of fracture Mechanics with boundary discontinuities or crack singularities.

In some model problems of linear elasticity, in the three-dimensional space, the governing equation is the so-called Beltrami-Michel equation of a three-variable function, which is known as "stress invariant" and is a function of the body forces each one acting along *x*, *y* or *z* axis:

$$\nabla^2\sigma_{ij} + \frac{1}{1+\nu}\frac{\partial^2\left(\sum_{k=1}^{3}\sigma_{kk}\right)}{\partial x_i \partial x_j} = -\frac{\nu}{1-\nu}\delta_{ij}\left(\sum_{k=1}^{3}\frac{\partial f_k}{\partial x_k}\right) - \left(\frac{\partial f_i}{\partial x_j} + \frac{\partial f_j}{\partial x_i}\right) =$$

$$= -\frac{\nu}{1+\nu}\delta_{ij}\nabla^2 Q_1 - \left(\frac{\partial f_i}{\partial x_j} + \frac{\partial f_j}{\partial x_i}\right) \quad i, j = 1,2,3 \tag{1}$$

where ν is the Poisson ratio, σ_{ij} are the stresses, Q_1 is the first stress invariant and f_1, f_2 and f_3 are body forces. In some problems body forces are constant and thus the above equation is deduced to the following form:

$$\nabla^2\sigma_{ij} + \frac{1}{1+\nu}\frac{\partial^2\left(\sum_{k=1}^{3}\sigma_{kk}\right)}{\partial x_i \partial x_j} = \nabla^2\sigma_{ij} + \frac{1}{1+\nu}\frac{\partial^2 Q_1}{\partial x_i \partial x_j} = 0 \tag{2}$$

Thus, according to the compatibility condition, the governing equation is $\Delta(Q_1) = 0$. But it is well known that complexities appear when there are boundary singularities which form a particular type of problems.

In engineering mechanics, this type of problems is of great importance because boundary singularities affect seriously the regularity of the solutions, leading to convergence irregularities and low accuracy which is dispersed in all the domain of the problem. During the last decade of the 20th century several techniques have been developed (e.g., Aliabadi and Rooke 1991, Li 1998) aiming to efficiently and effectively tackle this category of problems. In many applications it is important to know in advance the values of the coefficients of all the leading terms appearing in the local solution, which is expressed in series form (Costabel et al. 2003, Szabo and Yosibash 1996) because they are related to other important parameters found in Fracture Mechanics (Aliabadi and Rooke 1991), such as the Mode III FMP. Obviously, knowledge of the values of these parameters enables the designers and engineers to decide about the appropriate materials and dimensions to use according to the anticipated loading and thermal conditions of the structure. In addition, it is also important to have a good knowledge of the type

of boundary singularities, in order to tackle them in the most appropriate way (Fung 1977). In two-dimensional elliptic boundary value problems sometimes appear two types of boundary singularities (Figure 1). The first type is a discontinuity in the boundary conditions (an abrupt change in the boundary conditions around a point) mainly caused by a crack. The second type is a re-entrant corner.

Figure 1. *Two Types of Planar Singularities*

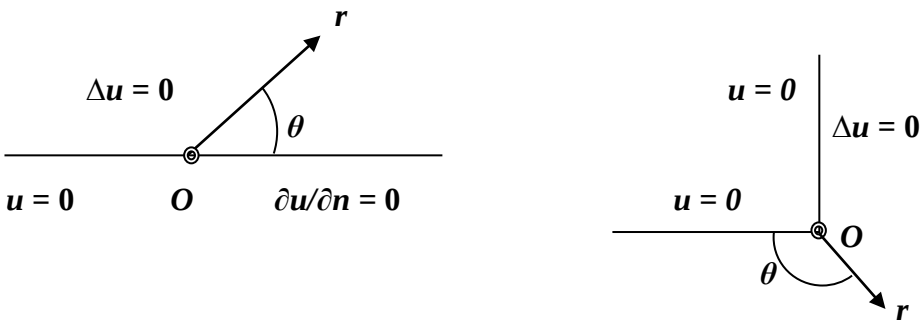

The local solution, in the neighborhood of the singularity of a two-dimensional problem, is expressed in the form of an asymptotic expansion in terms of the singular coefficients a_j which are the primary unknowns:

$$u = \sum_{j=1}^{\infty} a_j r^{\mu_j} U_j(\theta) \tag{3}$$

where $U_j(\theta)$ is the singular function and μ_j are the eigen-values of the problem.

A large number of numerical techniques, which appear in the literature, are based on post-processing of the numerical solution, such as the *p-hp* Finite Element Method or other finite element schemes (Seshaiyer and Suri 1998, Stephan and Whiteman 1988, Brannick et al. 2008, Brenner 1999, Brenner and Scott 1994) the accuracy and convergence rate of which are not adequate enough. However, the general idea of these methods is that the boundary singularity is considered in the design of the finite element grid by employing an appropriate refinement and the values of the coefficients of the local solution are extracted by implementing post-processing, something which is not required with boundary element methods. The latter were initially developed to tackle planar problems and they do not require complicated grids. Also, they are applied on the boundary of the domain (Karageorghis 1992, Katsikadelis 1991).

The so-called Trefftz methods (Bernal and Kindelan 2010, Li et al. 2007, Li et al. 2008) belong to this type of mesh-less numerical techniques and are based on local solutions (e.g., equation (3)) or basis functions which satisfy the governing

equations and thus allow collocation to be conducted only on the boundary. These are the main characteristics of this category of methods which make them more appropriate than the post-processing methods. In Li et al. (2008) it is explained that the main advantages of the Trefftz methods over the FEM and finite difference methods, include their flexibility in representing the boundary singularities and irregular geometry of the problem domains, ease of data input and pre-processing, high accuracy of the numerical solution and efficient computation. In the same reference it is mentioned that especially for the collocation Trefftz method (CTM) it has been shown that it is a more accurate numerical technique compared with other numerical methods (including the post-processing methods) not only for the global solution but also for the leading coefficients of the local solution expansion, something which is important in problems of Fracture Mechanics.

The singular function boundary integral method (SFBIM) is a Trefftz method and is used in the present work. Its fundamental characteristic is that the solution is approximated by the leading terms of the local asymptotic series around the boundary singularity. It has been developed by G. Georgiou and co-workers and has been used in many studies to tackle planar harmonic and biharmonic equation problems and three-dimensional Laplace equation problems in the fields of theoretical and fracture Mechanics, fluid flow, etc. (Christodoulou et al. 2012a, b, Elliotis et al. 2010, Elliotis et al. 2002, Elliotis et al. 2005a, b, Elliotis et al. 2006, Elliotis et al. 2007, Elliotis et al. 2014, Elliotis 2016, Elliotis 2019, Georgiou et al. 1996, Xenophontos et al. 2006). It exhibits exponential convergence, a feature which was observed in all previous applications of the method. Its application in three-dimensional problems (Christodoulou et al. 2012b, Elliotis et al. 2010, Elliotis 2016), has given much encouragement to extend the method to other three-dimensional Laplacian problems of perfectly elastic solid bodies with a crack singularity. Also, in the last five or six years, researchers have worked on problems of Fracture Mechanics with crack singularities and have obtained interesting results (Yosibash and Mittelman 2016, Schapira and Yosibash 2020, Omer and Yosibash 2019, Yosibash and Schapira 2021, Chaumont-Frelet and Nicaise 2018, Dauge and Nicaise 2017, Woo and Kim 2018). Following the same research interests, in the present work, we also examine the behavior of solid bodies when they develop a specific failure mode of Fracture Mechanics.

It is well known that in Fracture Mechanics there are three failure Modes (Aliabadi and Rooke 1991): Mode I (opening Mode), Mode II (in-plane shear Mode) and Mode III (out-of-plane shear Mode) which is the failure type examined in the current research (Figure 2). There is a very rich literature around these failure Modes in which the stress intensity factors play an important role in engineering analysis and calculations for the design of structures. In the present study we are interested in Failure Mode III.

Figure 2. *The Three Types of Failure Modes in Fracture Mechanics*

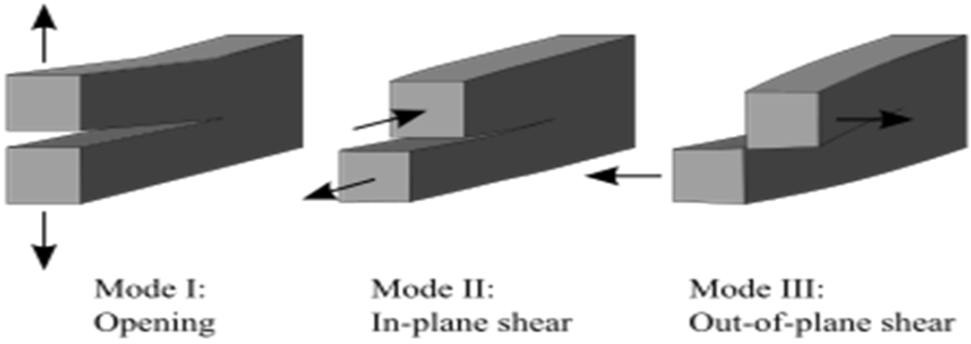

The rest of the article is organized as follows: in the next section a general 3-D Laplace equation problem of a solid body made of steel, with a crack singularity and a specific 3-D model problem of a steel rivet with a surface V-notch (singularity) are presented. Then, the general form of the local solution is given and the three-dimensional version of the SFBIM formulation, for the general and specific model problems, is presented. Numerical results are presented and discussed afterwards. Finally, in the last section, the conclusions are summarized.

The goal of this article is to present the extension of the SFBIM in Fracture Mechanics to efficiently solve the two problems of solid bodies, with a surface crack singularity (V-notch), exhibiting a failure Mode III. Also, the objective of the present study is to prove that, for the specific two problems, this method is much faster (i.e., it requires much smaller CPU time) and is much more accurate than the finite element method (FEM) which is still widely used by engineers and researchers by employing commercial packages. The novelty in the present study is that the SFBIM is extended in 3-D problems of Fracture Mechanics, exhibiting great advantages over the FEM. This encourages a further extension in this field of Mechanics.

General and Specific Model Problems

General Model Problem

In Figure 3 a general 3-D model problem of a solid body is presented. It has a straight-edge crack-singularity which is created by the intersection of two flat boundary parts S_A and S_B. In fact, this singularity is a straight line parallel to the Z-axis and at a distance d_c from this axis. The value of d_c can be varied. Both boundaries S_A and S_B form an angle φ_A with the XZ plane (i.e., S_B is symmetric to S_A with respect to the XZ plane). The external angle ω_d (as shown in Figure 3), between these two boundary parts, takes values in a certain range of values $[0.0002\pi, 1.9998\pi]$. Both ω_d and φ_A are measured in a local polar coordinate system (r, θ), with center O_d on boundary part S_D or K_d on S_E. Any other center of a local polar coordinate system, on a cross-section parallel to S_D and S_E, lies on the straight-edge crack-singularity. Flat boundaries S_D and S_E, on each one of the two

ends of the solid body, are vertical to both the *Z*-axis and the edge singularity and located at a distance *L* between them. The domain of the problem is also bounded by a boundary part S_C. It forms the cylindrical shape of the solid of the problem which has a cross-section with a circumference represented by the equation of an ellipse (Figure 3). Certainly, it retains a constant shape along *Z*-axis.

Figure 3. *Schematic Illustration of the Domain of the General Model Problem*

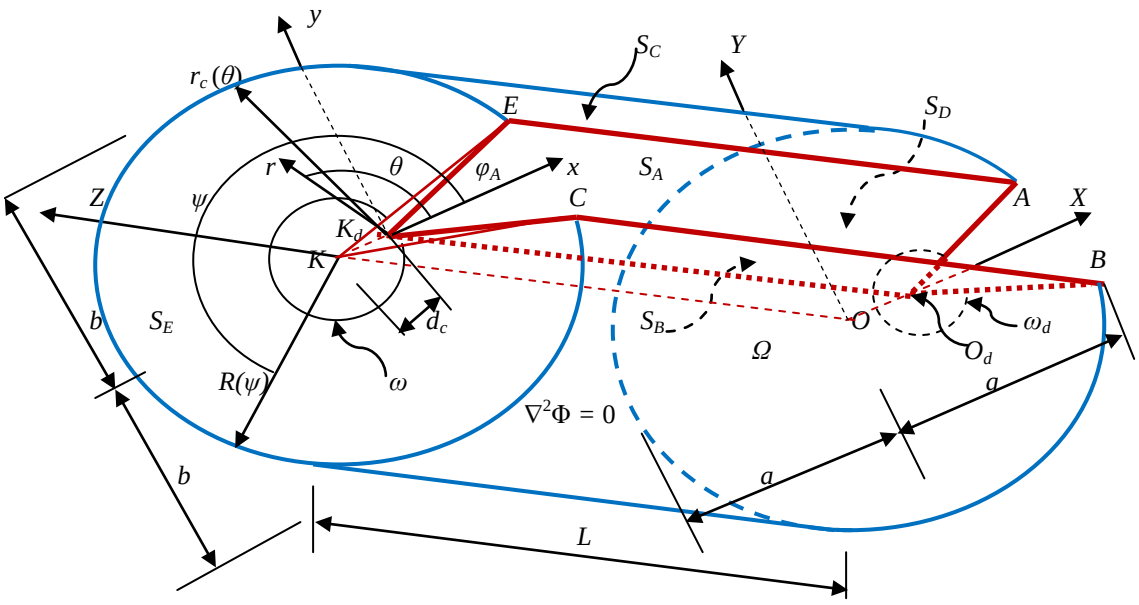

In Figure 3 the fundamental parameters ψ and $R[\psi(\theta)]$, employed in this problem, for the cylindrical co-ordinates, are defined as follows:

$$\psi = tan^{-1}\left(\frac{r_c(\theta)\,sin(\theta)}{d_c + r_c(\theta)\,cos(\theta)}\right), \qquad R[\psi(\theta)] = \frac{ab}{\sqrt{a^2\,sin^2[\psi(\theta)] + b^2\,cos^2[\psi(\theta)]}} \tag{4}$$

where *a* and *b* are the dimensions of the two axis of the elliptic cross-section.

The material of this solid body is isotropic homogeneous and obeys to Hooke's law. Also, there are no body forces. Thus, there is a scalar function $\Phi_g(r,\theta,z)$, known as Lamé strain potential function, which reduces the linear elasticity equations to the Laplace operator and is always independent of the values of Young's modulus *E* and the Poisson ratio *v* of the material (Fung 1977). Also, as per Fung (1977), the potential function generates the field of stresses (stress tensor). According to the same reference, which is one of the known classical books about theoretical Mechanics, stresses σ_{rr}, $\sigma_{\theta\theta}$, σ_{zz}, $\sigma_{r\theta}$, $\sigma_{\theta z}$ and σ_{zr} and displacements ξ_r, ξ_θ and ξ_z are expressed in cylindrical coordinates in terms of function $\Phi_g(r,\theta,z)$ as follows (with *G* being the shear modulus and defined as $G = \frac{E}{2(1+\nu)}$):

$$\begin{aligned}
&\sigma_{rr} = \partial_r^2 \Phi_g, && \sigma_{\theta\theta} = r^{-1}\partial_r \Phi_g + r^{-2}\partial_\theta^2 \Phi_g, && \sigma_{zz} = \partial_z^2 \Phi_g \\
&\sigma_{r\theta} = \partial_r\left(r^{-1}\partial_\theta \Phi_g\right), && \sigma_{\theta z} = r^{-1}\partial_\theta\left(\partial_z \Phi_g\right), && \sigma_{zr} = \partial_z\left(\partial_r \Phi_g\right) \\
&\xi_r = (1/2G)\partial_r \Phi_g, && \xi_\theta = (1/2G) r^{-1}\partial_\theta \Phi_g, && \xi_z = (1/2G)\partial_z \Phi_g
\end{aligned} \quad (5)$$

The mathematical conditions can be derived from the physical conditions of the problem. Thus, the mathematical problem is expressed as follows: Find $\Phi_g(r,\theta,z)$ such that

$$\nabla^2 \Phi_g = \Delta \Phi_g = 0 \quad in \quad \Omega \quad (6)$$

with the following physical and mathematical conditions:

$$\left.\begin{array}{lll}
\sigma_{\theta\theta}(r,z) = 0 & or \quad \Phi_g = 0 & on \quad S_A \\
\xi_\theta(r,z) = 0 \ (no\ distortion) & or \quad \partial_\theta \Phi_g = 0 & on \quad S_B \\
\sigma_{rr} = p(\theta,z) = \partial_r^2(\Phi_g(r,\theta,z))\big|_{r\to R(\theta)} & or \quad \Phi_g = f_g(\theta,z) & on \quad S_C \\
\delta_D(r,\theta) = \xi_z\big|_{S_D} = -\xi(r,\theta), & or \quad \partial_z \Phi_g = -2G\xi(r,\theta) & on \quad S_D \\
\delta_E(r,\theta) = \xi_z\big|_{S_E} = \xi(r,\theta), & or \quad \partial_z \Phi_g = 2G\xi(r,\theta) & on \quad S_E
\end{array}\right\} \quad (7)$$

Lamé potential $\Phi_g(r,\theta,z)$ is not known for this general model problem with boundary singularity. The expressions of functions $f_g(\theta,z)$ and $\xi(r,\theta)$ are as follows:

$$f_g(\theta,z) = \Phi_g(r,\theta,z)\big|_{r\to r_c(\theta)} = \sum_{k=1}^{2}\left[\sum_{j=1}^{2} a_{k,j} z^{j-1}\right] r_c(\theta)^{\frac{(2k-1)\pi}{2(\omega_d-\varphi_A)}} \sin\left(\frac{(2k-1)\pi}{2(\omega_d-\varphi_A)}\varphi(\theta)\right), \quad (8)$$

$$\varphi_A \le \theta \le \omega_d, \quad \omega_d = 2\pi - 2\varphi_A$$

$$\xi(r,\theta) = \frac{1}{2G}\sum_{k=1}^{2}\left[\partial_z\left(\sum_{j=1}^{2} a_{k,j} z^{j-1}\right)\right] r^{\frac{(2k-1)\pi}{2(\omega_d-\varphi_A)}} \sin\left(\frac{(2k-1)\pi}{2(\omega_d-\varphi_A)}(\theta-\varphi_A)\right) \quad (9)$$

Specific Model Problem of a Steel Rivet with a Surface V-notch

The general model problem discussed in the previous subsection is now specialized into a model problem of a solid body schematically illustrated in Figure 4. As a special case of the more general problem of the previous sub-section, the values of *a* and *b* (Figure 3) are now equal to each other and each point of the circumference of any circular cross section, on cylindrical boundary S_C, is at equal distance from the *z*-axis. The solid body of this particular model problem is a metal rivet with a circular cross section of radius R=1cm, which connects three steel members of a structure to create a joint. Its middle part has a length L=2 cm and is transmitting an eccentric load which comes from the middle element. Thus, its cylindrical surface is subjected to a distributed load $q(\theta,z)$ which is acting along the radial direction and is expressed in *MPa* (a common unit of pressure).

Figure 4. *Schematic Illustration of the 3-D Image and Layout of Joint (Specific Model Problem of a Steel Rivet with a V-notch)*

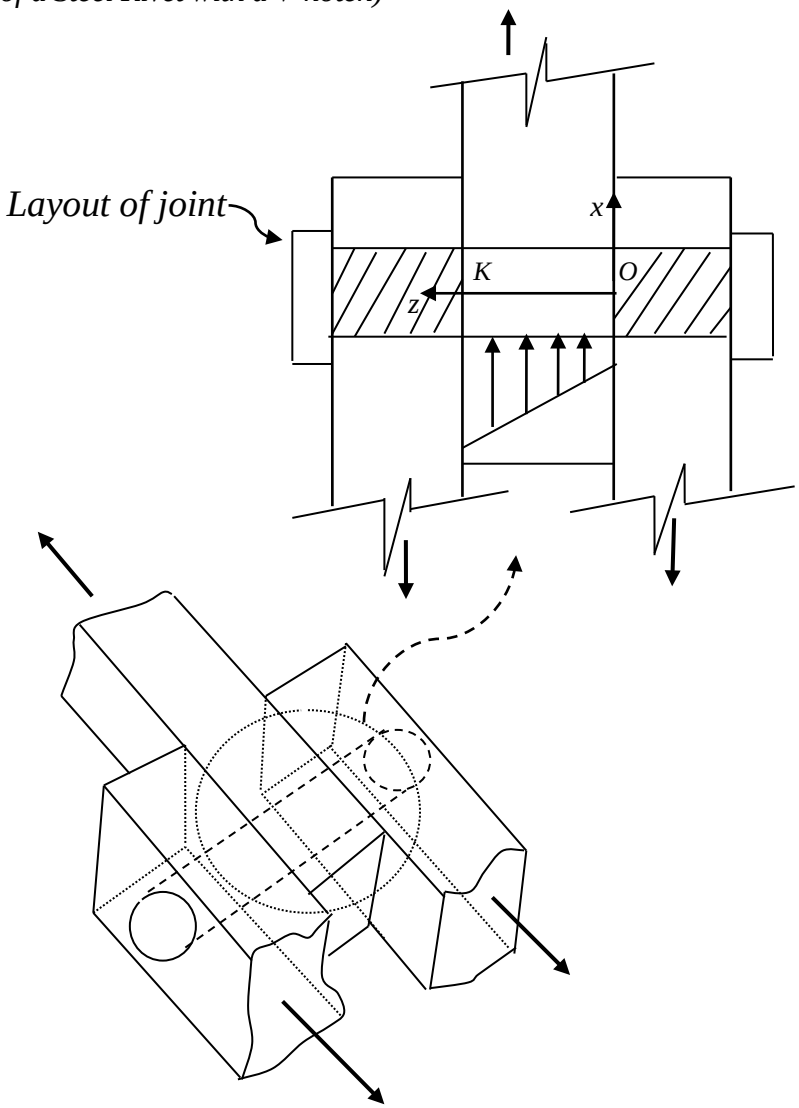

There is a crack on this solid body, represented by a V-notch which can propagate under certain stress and strain concentration states and in general has its vertex on a line parallel to the axis of the cylinder (z-axis) at a distance d_c. In the current work it is investigated whether the applied loading activates crack propagation. As we will see, after several numerical experiments, distance d_c is finally taken equal to zero. This choice is made in order to study the worst case of crack formation of Mode III in the steel rivet of this specific problem. Engineering experience indicates that under certain loading conditions further crack propagation, in this particular case, most probably leads the material to a failure (Aliabadi and Rooke 1991), something which will be also examined in the present study together with other material properties. Together with the distributed load there is a displacement $\xi(r,\theta)$ which takes place along the *z*-axis on each one of the cross

sections at positions *K* and *O* (Figure 4). The self-weight of the body is negligible compared with other loads and is ignored. Therefore, there are no body forces.

According to the description of the physical problem given above, the principal physical boundary conditions are as follows:

$$\left.\begin{array}{ll} \sigma_{\theta\theta} = 0, & on \quad S_A \\ \xi_\theta = 0, & on \quad S_B \\ \sigma_{rr} = q(\theta, z), & on \quad S_C \\ \xi_z\big|_{S_D} = -\xi(r,\theta), & on \quad S_D \\ \xi_z\big|_{S_E} = \xi(r,\theta), & on \quad S_E \end{array}\right\} \tag{10}$$

where the stresses σ_{rr}, $\sigma_{\theta\theta}$ and σ_{zz} and the displacements ξ_θ and ξ_z can be easily deduced from $\Phi_s(r,\theta,z)$ which is known for this problem (Fung 1977) and is expressed in cylindrical coordinates. Considering boundary conditions (10) the problem is specialized as follows: Find Φ_s such that

$$\nabla^2\Phi_s = \Delta\Phi_s = \partial_r^2\Phi_s + r^{-1}\partial_r\Phi_s + r^{-2}\partial_\theta^2\Phi_s + \partial_z^2\Phi_s = 0 \quad in \quad \Omega \tag{11}$$

$$\left.\begin{array}{ll} \Phi_s = 0, & on \quad S_A \\ \partial_\theta\Phi_s = 0, & on \quad S_B \\ \Phi_s = f_s(\theta, z) & on \quad S_C \\ \partial_z\Phi_s = -\zeta(r,\theta), & on \quad S_D \\ \partial_z\Phi_s = \zeta(r,\theta), & on \quad S_E \end{array}\right\} \tag{12}$$

where $\zeta(r,\theta) = 2G\xi(r,\theta)$. Also, for $d_c \neq 0$ functions $f_s(\theta,z)$, $\zeta(r,\theta)$, $\Phi_s(r,\theta,z)$ and $q(\theta,z)$ have the following mathematical expressions:

$$f_s(r,\theta,z)\big|_{r\to r_c(\theta)} = \sum_{k=1}^{2}\left[\sum_{j=1}^{2} a_{k,j} z^{j-1}\right] r^{\frac{(2k-1)\pi}{2(\omega_d-\varphi_A)}} \sin\left(\frac{(2k-1)\pi}{2(\omega_d-\varphi_A)}(\theta-\varphi_A)\right)\Bigg|_{r\to r_c(\theta)}$$

$$where \quad r_c(\theta) = \left[\sqrt{R^2 - d_c^2\sin^2(\theta)} - d_c\cos(\theta)\right]_{R\to 1\,cm} \tag{13}$$

$$\zeta(r,\theta) = -\partial_z\Phi_s\big|_{s_D} = \partial_z\Phi_s\big|_{s_E} = 2\left[r^{\frac{\pi}{2(\omega_d-\varphi_A)}}\sin\left(\frac{\pi(\theta-\varphi_A)}{2(\omega_d-\varphi_A)}\right) + r^{\frac{3\pi}{2(\omega_d-\varphi_A)}}\sin\left(\frac{3\pi(\theta-\varphi_A)}{2(\omega_d-\varphi_A)}\right)\right] \tag{14}$$

$$\Phi_s(r,\theta,z) = (1+2z)\left[r^{\frac{\pi}{2(\omega_d-\varphi_A)}}\sin\left(\frac{\pi(\theta-\varphi_A)}{2(\omega_d-\varphi_A)}\right) + r^{\frac{3\pi}{2(\omega_d-\varphi_A)}}\sin\left(\frac{3\pi(\theta-\varphi_A)}{2(\omega_d-\varphi_A)}\right)\right], \tag{15}$$

$$q(\theta,z) = \partial_r^2(\Phi_s(r,\theta,z))\big|_{r\to r_c(\theta)} \tag{16}$$

Note that all values of boundary conditions are dimensional: distributed loads are expressed in N/cm^2 and lengths in *cm* and can be easily converted into *MPa* and *m* respectively, which are common units in most engineering problems. As already mentioned, when parameter d_c is taken equal to zero it is $\omega_d=\omega$ and $r_c(\theta)=R=1$ *cm* and on any cross-section angle θ is measured from an axis parallel to the *x*-axis (Figure 5). Then for this specific case the above expressions take the following form (they can be also expressed in the Cartesian coordinate system but here they are expressed in the cylindrical coordinate system centered at the *z*-axis as shown in Figure 5):

$$q(\theta,z)=\partial_{rr}\left(f_s(r,\theta,z)\right)\Big|_{r\to 1\ cm}= \\ =(1+2z)\frac{\pi}{2\omega}\left[\left(\frac{\pi}{2\omega}-1\right)\sin\left(\frac{\pi\theta}{2\omega}\right)+3\left(\frac{3\pi}{2\omega}-1\right)\sin\left(\frac{3\pi\theta}{2\omega}\right)\right] \tag{17}$$

$$f_s(r,\theta,z)\Big|_{r\to 1\ cm}=(1+2z)\left[\sin\left(\frac{\pi\theta}{2\omega}\right)+\sin\left(\frac{3\pi\theta}{2\omega}\right)\right] \tag{18}$$

$$\zeta(r,\theta)=-\partial_z\Phi_s\Big|_{S_D}=\partial_z\Phi_s\Big|_{S_E}=2\left[r^{\frac{\pi}{2\omega}}\sin\left(\frac{\pi\theta}{2\omega}\right)+r^{\frac{3\pi}{2\omega}}\sin\left(\frac{3\pi\theta}{2\omega}\right)\right] \tag{19}$$

$$\Phi_s(r,\theta,z)=(1+2z)\left[r^{\frac{\pi}{2\omega}}\sin\left(\frac{\pi\theta}{2\omega}\right)+r^{\frac{3\pi}{2\omega}}\sin\left(\frac{3\pi\theta}{2\omega}\right)\right] \tag{20}$$

Figure 5 depicts the mathematical form of this model problem and presents, mainly, its geometrical characteristics and the mathematical domain Ω_s of the above problem. Angle ω presented in the figure has maximum and minimum values equal to 1.998π *rads* and 0.002π *rads* respectively. Note that for very small values, such as $\omega=0.002\pi$ *rads*, the solid body becomes a blade. Also, in Figure 5, the schematic illustration of the distribution of the resulting surface tractions $q(r,\theta)$ on boundary S_C is presented. The distribution of surface traction at a cross section with $z=1$ cm, is also presented in the same figure. This external load distribution, which can be determined from the known solution, indicates that external loading on the solid body is not symmetric and causes bending to the central part of the rivet. Thus, apart from $q(r,\theta)$ additional stresses due to friction (shear stresses) and contact of the rivet with the middle steel member, appear on S_C.

Figure 5. *Specific Model Problem's Domain with Schematic Illustration (not to Scale)*

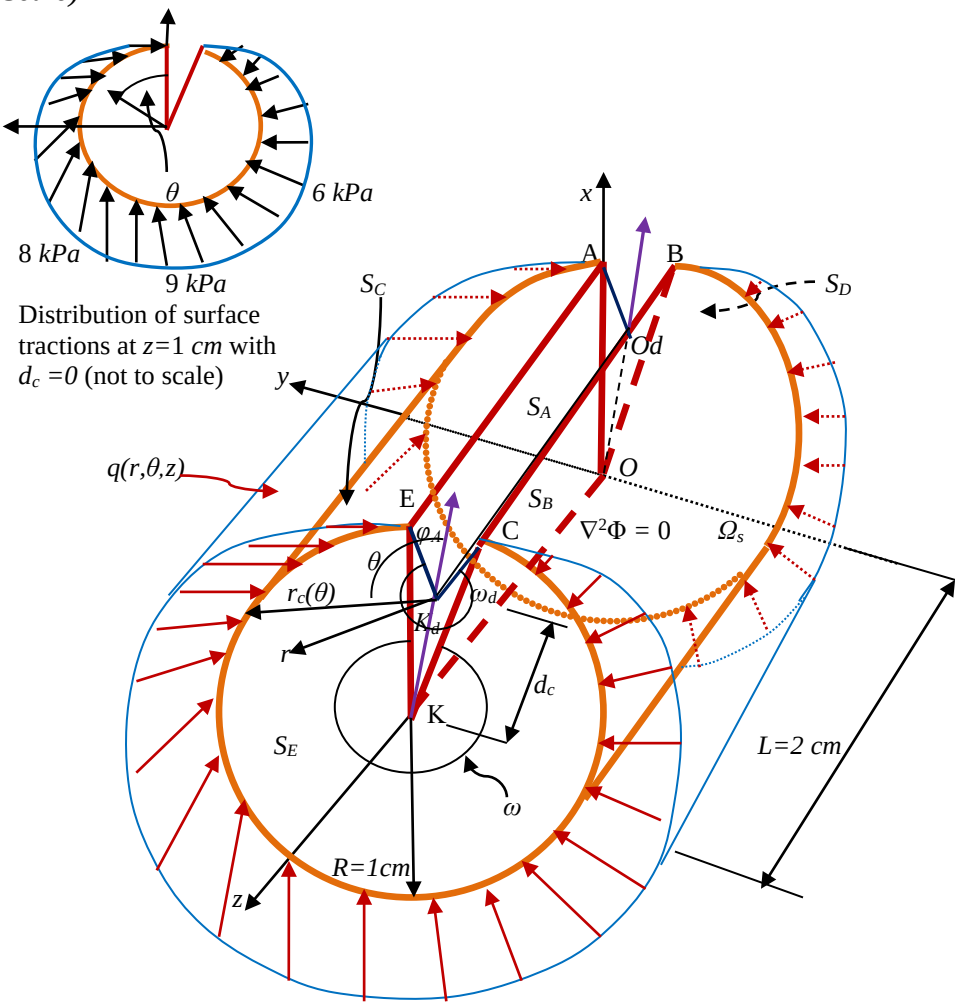

For this problem it is E=210GPa and ν=0.30. Also, the material of the solid body is a high-yield steel of type S700MC, suitable for cold forming structural load-bearing components, with a titanium content of 0.22% and yield strength (elastic limit) σ_y=620MPa. Beyond this limit, elastic-plastic deformation appears.

A Boundary Integral Method in 3-D

Formulation of the Method

The solution Φ of the 3-D Laplace equation, is expressed in cylindrical coordinates and is defined in a domain with a boundary crack singularity along the z-axis or along a line parallel to this axis, as it is the case of the model problems which have been examined in the current study. It is written as follows (Costabel et al. 2003, Christodoulou et al. 2012b, Elliotis et al. 2010, Elliotis 2016):

$$\Phi(r,\theta,z)=\sum_{k=1}^{\infty}\left[\left(F^{(a_k)}(z)+\sum_{i=1}^{\infty}c_{k,i}\partial_z^{2i}\left(F^{(a_k)}(z)\right)r^{2i}\right)r^{a_k}\varphi_k(\theta,a_k)\right], \qquad (21)$$

In the present work, function Φ represents the Lamé strain potential function (Fung 1977) as has already been mentioned. The mixed boundary conditions on the boundary parts S_A and S_B, which share the boundary singularity, do not yield logarithmic terms in (21) because eigenvalues α_κ are not integers and there are no "crossing points". Although both the general and specific model problems in Figures 3 and 5, have mixed boundary conditions on boundaries S_A and S_B which share the singularity, it is known that for the isotropic materials in 3-D linear elasticity, which is the case of our problems, the local solution expansion in the vicinity of the singularity does not contain any logarithmic terms (Costabel et al. 2003).

In elliptic coordinates, as it is the case of the general model problem, the singular solution may be found by following the theory developed in Li et al. 2008. According to the same reference the elliptic coordinates fail to present the concave corners with $\theta<2\pi$. Thus, we have to solicit the singular solution in cylindrical coordinates. Moreover, for the general model problem and as per Li et al. (2007) and Li et al. (2008), expression (21) is preferred for simplicity. Now, in (21) functions $F^{(a_k)}(z)$ are polynomials of degree N_p and with unknown coefficients $a_{k,j}$ and are expressed as follows:

$$F^{(a_k)}(z)=\sum_{j=1}^{N_p+1}\alpha_{k,j}z^{j-1} \qquad (22)$$

The eigenfunctions $\varphi_\kappa(\theta,\alpha_\kappa)$ and the eigenvalues α_κ in (21) are given by

$$\varphi_k(\theta,a_k)=\sin(a_k(\theta-\varphi_A)),\quad a_k=((2k-1)\pi)/(2(\omega_d-\varphi_A))\quad k=1,2,\cdots \qquad (23)$$

where ω_d is shown in Figures 3 and 5. Also, for the specific model problem the first two functions $F^{(a_k)}(z)$ are known and they are of the form ($a_{k,j}$ are known):

$$F^{(a_k)}(z)=1+2z,\quad \text{for } k=1 \text{ or } 2. \qquad (24)$$

which means that $N_p=1$. For the general model problem, polynomials $F^{(a_k)}(z)$ are not known.

With the SFBIM, the solution of the model problems analyzed is approximated by the leading N_a terms of the local asymptotic expansion (21):

$$\overline{\Phi}(r,\theta,z)=\sum_{k=1}^{N_a}\left\{\sum_{j=1}^{N_p+1}a_{k,j}\underbrace{\left[z^{j-1}+\sum_{i=1}^{N}c_{k,i}\partial_z^{2i}\left(z^{j-1}\right)r^{2i}\right]r^{a_k}\sin\left(a_k(\theta-\varphi_A)\right)}_{V_k^{(j)}}\right\} \quad (25)$$

where the over-bar denotes an approximate quantity. In the above expansion, the inner function, denoted by $V_k^{(j)}$, is the so-called singular function, in which N is an additional parameter, selected so that $N_p<2N+1$, the latter being the result of the substitution of Φ, expressed by (25), into the governing equation (Elliotis 2016) and asking the expression to satisfy the 3-D Laplace equation. Also, parameter $c_{k,i}$ is defined as $c_{k,i}=(-1/4)^i/\left(\Pi_{l=1}^{i}l(\alpha_k+l)\right)$.

Following the standard procedure of the SFBIM for the 3-D case (Christodoulou et al. 2012b, Elliotis et al. 2010, Elliotis 2016), the governing equation is weighted by the singular functions $V_k^{(j)}$, in the Galerkin sense, to give $(N_p+1)N_a+N_\lambda$ discretized equations. Then, after applying Gauss divergence theorem and by considering that functions $V_k^{(j)}$ satisfy exactly the boundary conditions along S_A and S_B and also by imposing the Dirichlet boundary condition on S_C, by means of Lagrange multiplier $\mu(\theta,z)$, we finally arrive at the following linear system of $(N_p+1)N_a+N_\lambda$ discretized equations:

$$\iint_{S_C}\left(\mu V_k^{(j)}-\overline{\Phi}\left(\partial_n V_k^{(j)}\right)\right)dS+\iint_{S_D}\left(-\zeta V_k^{(j)}+\overline{\Phi}\left(\partial_n V_k^{(j)}\right)\right)dS+$$

$$+\iint_{S_E}\left(\zeta V_k^{(j)}-\overline{\Phi}\left(\partial_n V_k^{(j)}\right)\right)dS=0, \quad (26)$$

$$k=1,2,\cdots,N_a, \qquad j=1,2,\cdots,N_p+1$$

$$\iint_{S_C}\overline{\Phi}B_i\,dS=\iint_{S_C}q_s(\theta,z)B_i\,dS, \qquad i=1,2,\cdots,N_\lambda \quad (27)$$

In applying the SFBIM for the general model problem, equation (27) takes the form:

$$\iint_{S_C}\overline{\Phi}B_i\,dS=\iint_{S_C}p_g(\theta,z)B_i\,dS, \qquad i=1,2,\cdots,N_\lambda \quad (28)$$

In (26) Lagrange multiplier $\mu(\theta,z)$ is expanded in terms of bilinear basis functions $B_i(\theta,z)$:

$$\mu(\theta,z)=\partial_n\overline{\Phi}(r,\theta,z)=\sum_{i=1}^{N_\lambda}\mu^{(i)}B_i(\theta,z), \quad \text{with } r=R \text{ on } S_C \quad (29)$$

As in previous applications of the method, the nodal values of μ are the additional unknowns.

System of Discretized Linear Equations in Block Form

Integration is performed away from the boundary singularity *OD* which lies along the *z*-axis. This is an advantage for the procedure since the *z*-axis is a strong singularity. Furthermore, the system of discretized equations (26) and (27) or (28) is a system of linear equations in which $\Phi(r,\theta,z)$ and $\mu(\theta,z)$ are substituted by their expansions (25) and (29), respectively.

The coefficients of the unknowns $a_{k,j}$ and $\mu^{(i)}$ are represented by expressions with integrals which contain terms with $V_k^{(j)}$ and $B_i(\theta,z)$ and their derivatives. The system takes the form:

$$\begin{bmatrix} M_1 & M_2 \\ M_2^T & M_0 \end{bmatrix} \cdot \begin{bmatrix} \mathrm{X} \\ \Lambda \end{bmatrix} = \begin{bmatrix} C_0 \\ C_C \end{bmatrix} \qquad (30)$$

where vector X contains the first set of unknowns $a_{k,j}$ and vector Λ contains the second set of unknowns $\mu^{(i)}$. Sub-matrix M_0 and vector C_0 contain zeros. System (30) is solved by using the Gauss elimination procedure. Obviously, the stiffness matrix is symmetric and it becomes singular or ill-conditioned (Xenophontos et al. 2006) when $(N_p+1)N_a<N_\lambda$ in which case the method diverges.

Numerical Results

For the estimation of integrals (26), (27) and (28) for both the general and specific model problems, numerical integration takes place on all boundary parts, except from S_A and S_B. For example, the calculation of integrals on S_C is performed by applying $N_E=N_z\times N_\theta$ boundary elements on this boundary part. Integration takes place on each element by using a 3×3 Gauss-Legendre quadrature rule. The boundary elements grid and the shape of basis functions are presented in Figure 6.

Figure 6. *Grid of Boundary Elements and Shape of Basis Functions*

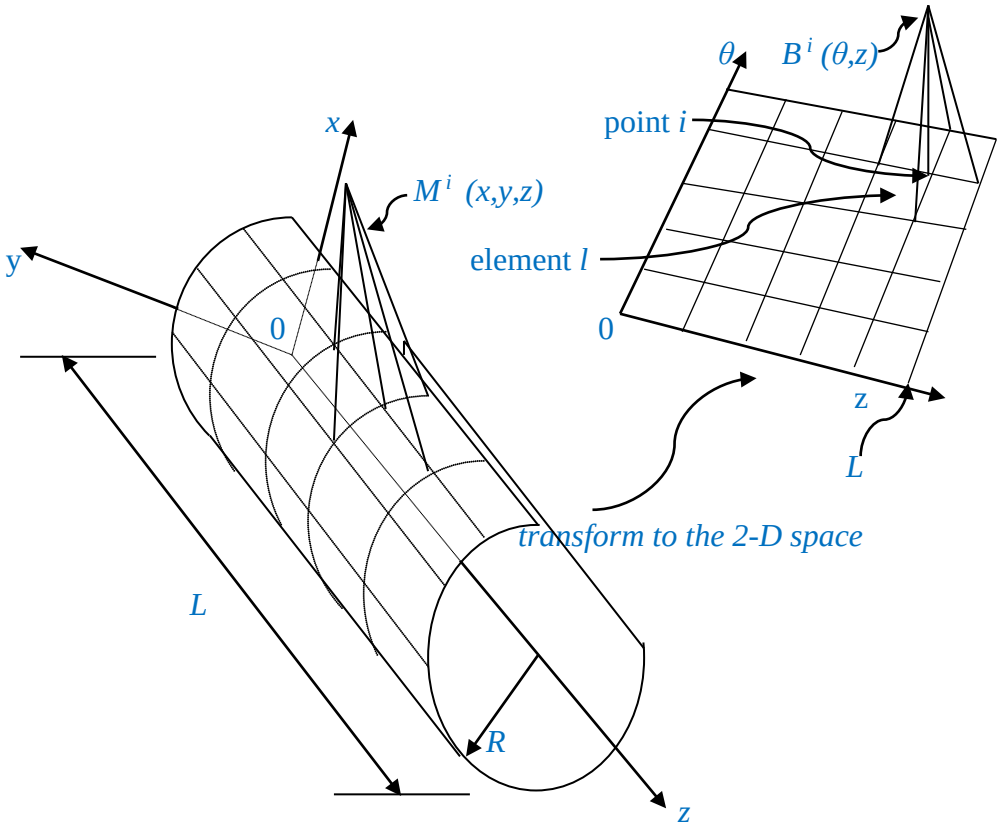

Table 1 presents the converged values of the leading singular coefficients $a_{k,j}$ corresponding to the general model problem obtained with both the SFBIM and the FEM, for a specific value of d_c (distance between the edge singularity and the *z*-axis as indicated in Figure 5) and for a specific value of small axis *b* (see the elliptic cross-section in Figure 3). Thus, as the value of the big axis *a*, on the elliptic cross-section, varies, different values of singular coefficients are obtained at convergence in using the SFBIM. It must be noted that with the method, convergence occurs for a specific combination of $(N_p+1)N_a$, in number, singular coefficients and of N_λ Lagrange multipliers. Also, the CPU time has been recorded for both the SFBIM and the FEM. One may easily observe that the SFBIM is much more accurate and much faster than the FEM.

Table 1. *Converged Values of the Leading Singular Coefficients $a_{k,j}$ of the General Model Problem, Obtained with the SFBIM and the FEM for d_c=0.6 cm and b=1.5 cm*

L (cm)	*a/b*	ω_d *(rads)*	*Leading singular coefficients* $a_{k,j}$ *k*	*j*	**SFBIM** average CPU time per run = 0.6 sec	**FEM** (with grid refinement) average CPU time per run= 22.7 sec
			1	1	1.0000000000000012	1.0004
		0.1998π	1	2	2.0000000000000014	1.9997
		:	2	1	1.0000000000000013	0.9995
		:	2	2	1.9999999999999985	2.0003
	1.20		:	:	:	:
			:	:	:	:
		:	1	1	1.0000000000000057	0.9996
		1.9998π	1	2	1.9999999999999949	2.0002
0.1			2	1	1.0000000000000062	1.0004
	:	:	2	2	2.0000000000000077	2.0002
		:	:	:	:	:
	:		:	:	:	:
		:	1	1	1.0000000000000059	0.9997
	3.00		1	2	2.0000000000000073	2.0001
		1.9998π	2	1	1.0000000000000081	1.0003
			2	2	2.0000000000000064	2.0001
:	:	:	:	:	:	:
:	:	:	:	:	:	:
4.0		:	1	1	1.0000000000000069	1.0003
	3.00	:	1	2	2.0000000000000057	2.0002
		1.9998π	2	1	1.0000000000000074	1.0001
			2	2	2.0000000000000087	2.0001

Table 2 contains the converged values of the leading singular coefficients $a_{k,j}$ corresponding to the specific model problem, for a radius *R* of the rivet equal to 1 cm and for the case where the edge singularity coincides with the *z*-axis. These numerical results (converged values) were obtained by the SFBIM and for the "optimal" combination of the number of singular coefficients and Lagrange multipliers. Also, it is observed that the numerical error with the SFBIM is significantly less than the error which occurs in using the FEM. With Table 3 a comparison is made between the two methods for the values of the polynomial functions at *z*=1.0, regarding the specific model problem. Again, one may easily see how much faster and accurate is the SFBIM compared with the FEM employed together with grid refinement.

Table 2. *Converged Values of the Leading Singular Coefficients $a_{i,k}$, Regarding the Specific Model Problem, for R=1cm and for d_c=0 cm, with the SFBIM and the FEM*

k	j	$a_{k,j}^{(SFBIM)}$ (for "optimal" combination $(N_p+1)N_a=32$; $N_\lambda=16$; $N_p=3$; $N=2$)	$a_{k,j}^{(FEM)}$ (with grid refinement)	$a_{k,j}^{(exact)}$	*error with the SFBIM* $\lvert a_{k,j}^{(SFBIM)} - a_{k,j}^{(exact)} \rvert$ average CPU time per run = 0.4 sec	*error with the FEM* $\lvert a_{k,j}^{(FEM)} - a_{k,j}^{(exact)} \rvert$ average CPU time per run = 17.2 sec
1	1	1.0000000000000016	1.0003	1.0000	1.6×10^{-15}	3×10^{-4}
1	2	2.0000000000000021	1.9999	2.0000	2.1×10^{-15}	1×10^{-4}
2	1	1.0000000000000018	0.9997	1.0000	1.8×10^{-15}	3×10^{-4}
2	2	2.0000000000000031	2.0002	2.0000	3.1×10^{-15}	2×10^{-4}

Table 3. *Comparison Between the Exact Solution and the Values Obtained by the SFBIM and the FEM, for R=1, d_c=0 cm and z=1.0 cm, for the First Two Polynomial Functions $F^{(a_k)})(z)$ Regarding the Specific Model Problem*

k	$F_{SFBIM}^{(a_k)}$	$F_{FEM}^{(a_k)}$	$F_{exact}^{(a_k)}$	$\lvert F_{SFBIM}^{(ak)} - F_{exact}^{(a_k)} \rvert$	$\lvert F_{FEM}^{(ak)} - F_{exact}^{(a_k)} \rvert$
1	3.0000000000000037	3.0002	3.0000	3.7×10^{-15}	2×10^{-4}
2	3.0000000000000049	2.9999	3.0000	4.9×10^{-15}	1×10^{-4}

The efficiency of the method is depicted in the graph shown in Figure 7 where error is defined as

$$\varepsilon_k = \left| F^{(a_k)}(z) - \overline{F}^{(a_k)}(z) \right|_{z=1} \qquad k = 1 \text{ or } 2 \tag{31}$$

where $|.|_{z=1}$ is the absolute value of the difference between the exact and the approximate values of $F^{(a_k)}(z)$ at z=1, for d_c=0 and ω=1.9998π *rads*. Graph indicates very high accuracy and fast convergence of the SFBIM.

Figure 7. *Graph of Errors ε_1 and ε_2 for $F^{(a_1)}$ (Lower Line) and $F^{(a_2)}$ (Upper Line) at z=1*

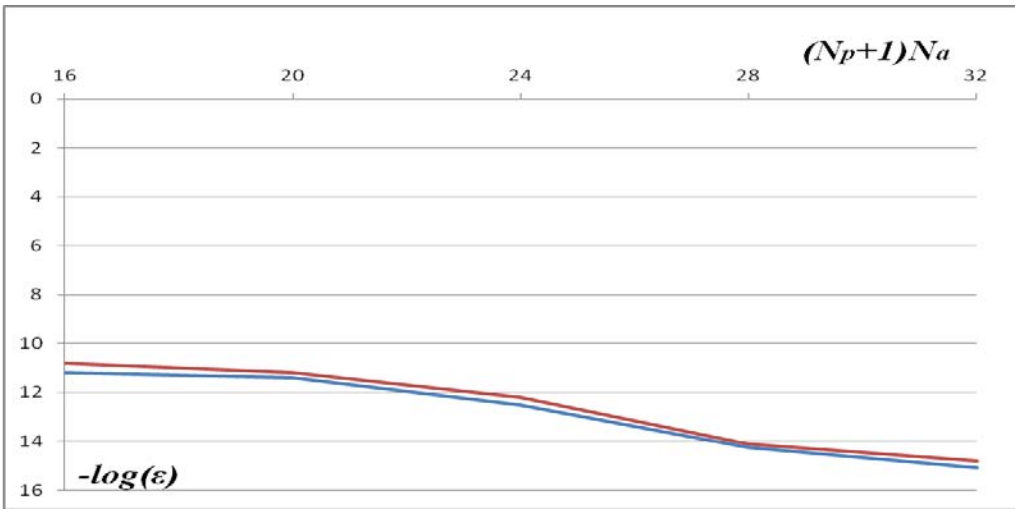

Having the numerical approximations of the singular coefficients, for the specific problem, the approximate function $\Phi_s(r,\theta,z)$ of the solution is now in complete form and the stresses at any point of the solid body (domain Ω_s with $d_c=0$ and thus $\omega_d=\omega$) at Figure 5, can be calculated from the following expressions in cylindrical coordinates (remember that eigen-values are $a_k=((2k\text{-}1)\pi)/(2\omega)$), in which index s is dropped:

$$\sigma_{rr} = \partial_r^2\overline{\Phi} \approx (1+2z)\sum_{k=1}^{2}\left[a_k(a_k-1)r^{a_k-2}\ sin(a_k\theta)\right] \tag{32}$$

$$\sigma_{\theta\theta} = r^{-1}\partial_r\overline{\Phi} + r^{-2}\partial_\theta^2\overline{\Phi} \approx -(1+2z)\sum_{k=1}^{2}\left[a_k(a_k-1)r^{a_k-2}\ sin(a_k\theta)\right] \tag{33}$$

$$\sigma_{zz} = \partial_z^2\overline{\Phi} \approx 0 \tag{34}$$

Note that in considering the series expansion of the above stresses it is always $\sigma_{rr}+\sigma_{\theta\theta}+\sigma_{zz}=0$ in all over domain Ω. This result is also deduced by adding stresses σ_{rr}, $\sigma_{\theta\theta}$, σ_{zz} which are expressed in terms of the potential. Also, the shear stresses are given by

$$\sigma_{r\theta} = \partial_r\left(r^{-1}\partial_\theta\overline{\Phi}\right) \approx (1+2z)\sum_{k=1}^{2}\left[a_k(a_k-1)r^{a_k-2}\ cos(a_k\theta)\right] \tag{35}$$

$$\sigma_{\theta z} = r^{-1}\partial_{z,\theta}^2\overline{\Phi} \approx 2\sum_{k=1}^{2}\left[a_k r^{a_k-1}\ cos(a_k\theta)\right] \tag{36}$$

$$\sigma_{zr} = \partial_{z,r}^2\overline{\Phi} \approx 2\sum_{k=1}^{2}\left[a_k r^{a_k-1}\ sin(a_k\theta)\right] \tag{37}$$

Table 4. *Values of Stresses at Position z=2 cm, with d_c=0 r=0.01 cm, at $\theta \approx 0$ and $\theta \approx \omega$*

Type of stress *(MPa)*	$\theta \to 0$	$\theta \to \omega$
σ_{rr}	0	-26.68
$\sigma_{\theta\theta}$	0	26.68
σ_{zz}	0	0
$\sigma_{r\theta}$	-32.58	0
σ_{rz}	0	0.11
$\sigma_{\theta z}$	0.21	0

Using the above expressions, the values for the stresses are obtained at z=2 cm, for θ=0 and for θ=ω, respectively, very near to the edge-singularity (r=0.01 *cm*) of problem's domain Ω_s. Position z=2 cm is chosen to have the greatest absolute values for all components of the stress tensor. These values are tabulated in Table 4.

Note that according to the theory of fracture Mechanics the mean value of the only out of plane displacement ξ_z and the values of stresses $\sigma_{\theta z}$ at $\theta \approx 0$ and σ_{rz} at $\theta \approx \omega$ are important for us since they help to arrive at the conclusion that the crack of the specific model problem (Figure 5) is of Mode III. Then one needs to calculate the Mode III FMP which is denoted by K_{III}. Stresses $\sigma_{\theta z}$ and σ_{rz} at $\theta \approx 0$ and $\theta \approx \omega$, respectively, are acting in the same direction but because $|\sigma_{\theta z}| \neq |\sigma_{rz}|$ there is a differential displacement between the two parts, on the left and on the right of the V-notch, along the length of the solid body. Thus, the crack is of Mode III. Parameter K_{III} is then calculated from (Aliabadi and Rooke 1991):

$$K_{III} = \lim_{r \to 0} \left(\sqrt{2\pi r}\, \sigma_{\theta z} \big|_{\theta = \frac{\omega}{2},\, z=2} \right) \qquad MPa.m^{1/2} \qquad (38)$$

Table 5 presents the values of $\sigma_{\theta z}$ in *MPa* and of K_{III} in $MPa.m^{1/2}$, with respect to r, calculated at the position with z=2 cm and θ=ω/2 and rounded to the 3rd decimal digit, as it is the custom in engineering applications. Also, Figure 8 depicts the behavior of K_{III} as r decreases. Since the material of the solid body of this problem is a high yield steel with a value of critical parameter $K_{III,c}$=50 $MPa.m^{1/2}$, then the largest of the values of K_{III}, which is obtained for the "nano-dimension" $r=10^{-7}$ cm (Table 5) indicates that there is no danger of crack propagation for the specific problem (i.e., $K_{III,max} < K_{III,c}$).

Table 5. *Values of the Stress Intensity Factor K_{III} for d_c=0 and for Different Values of r at z=2 cm and $\theta=\omega/2$*

r (*cm*)	$\sigma_{\theta z}$ (*MPa*)	*Mode III FMP* K_{III} ($MPa.m^{1/2}$)
10^{-2}	0.078	0.002
10^{-3}	0.570	0.005
10^{-4}	3.430	0.009
10^{-5}	19.657	0.016
10^{-6}	111.198	0.028
10^{-7}	626.230 (first yield)	0.049

Yielding (i.e., plastic deformation) does not take place anywhere in the material of the rivet, except from the area around the tip of the crack and within a cylindrical region of the material of radius $r=10^{-5}$ *cm*, in which plastic deformations and plastic strains (Fung 1977) take place (stress state exceeds the elastic limit but is confined within the plastic region which is formed around the singularity). Consequently, the solid body does not fail under the stress state and stress concentration in the region of the straight-edge singularity.

Figure 8. *Graphical Representation of Mode III Fracture Mechanics Parameter K_{III} for $d_c=0$ and at $z=2$ cm, $\theta=\omega/2$*

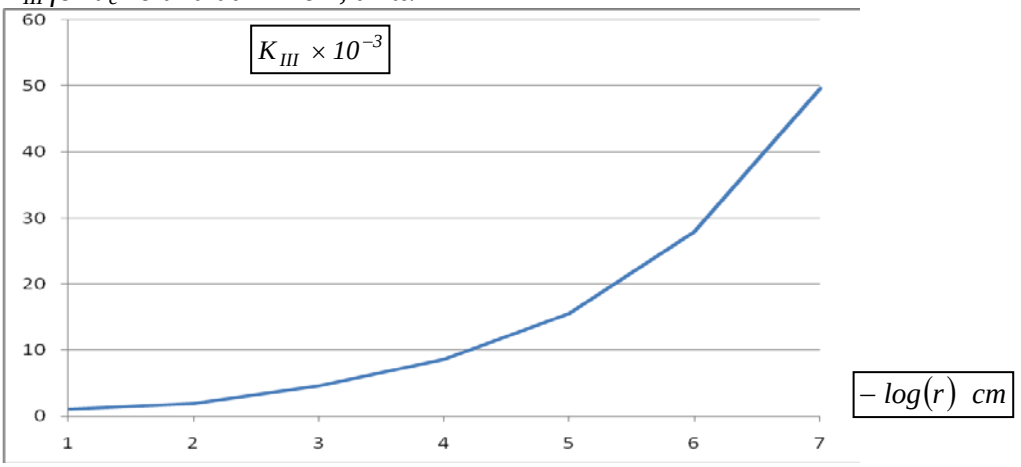

Conclusions

In this study two 3-D model problems are tackled. These are problems of linear elasticity in fracture Mechanics which are reduced to elliptic boundary value problems with a Laplacian governing equation of a Lamé potential. The first problem is a general model problem of a cylindrical body with a cross section in the form of an ellipse which retains its shape along the *z*-axis. The second model problem is a specific problem of a steel rivet (it could be also a steel bolt), with a circular cross section, which connects three elements of a structure. Both problems have a surface V-notch with a vertex which is treated as a boundary singularity.

The SFBIM, which is a Trefftz method, has been implemented in the current study and as in other previous applications of the method, very fast convergence and very high accuracy are achieved, in directly calculating the singular coefficients of the local solution expansion. Comparison between the results obtained for the values of the singular coefficients $a_{k,j}$ and the polynomial functions $F^{(a_k)}(z)$, with the SFBIM and the FEM (with grid refinement), shows that the latter is not as efficient as the SFBIM. Indeed, the numerical results indicate that our method presents much greater accuracy and much smaller computational time (smaller CPU time on the same computing machine) in compare to the FEM. The greater accuracy achieved by the method, is demonstrated by comparing the results of the two methods which were obtained in solving both the above general model problem (in which the exact solution is not available) and the above specific model

problem with a known solution. In fact, for both model problems, in implementing the SFBIM the mean value of the numerical error, at convergence, in all runs, is of the order of 10^{-15}, while for the FEM the corresponding error is about 10^{-4}.

Especially for the specific model problem, the results are also compared with the exact solution. Thus, the extension of this technique to both the general and the specific model problems is quite interesting, from the engineering point of view, since it constitutes a novel application of this specific methodology of applied mathematics in engineering. In particular, the capability of the method to tackle problems of Fracture Mechanics with crack discontinuities (boundary singularities) more efficiently and effectively in compare to the FEM with grid refinement, is demonstrated with the current study, something which encourages the implementation of its algorithm in subroutines of engineering packages to solve specific problems with boundary singularities, a domain in which other numerical schemes extract the values of the singular coefficients by post-processing the numerical solution.

As a general remark we would say that the application of the SFBIM to solve the above model problems, encourages its extension to other engineering problems with boundary singularities of a different type and with more complicated geometry and boundary conditions.

References

Aliabadi M, Rooke D (1991) *Numerical fracture mechanics*. United Kingdom: Kluer Academic Publishers.

Bernal F, Kindelan M (2010) Radial basis function solution of the Motz problem. *Engineering Comput*ations 27(Jul): 606–620.

Brannick JJ, Li H, Zikatanov LT (2008) Uniform convergence of the multi-grid V-cycle on graded meshes for corner singularities. *Numerical Linear Algebra with Applications* 15(2–3): 291–306.

Brenner SC (1999) Multigrid methods for the computation of singular solutions and stress intensity factors I: corner singularities. *Mathematics of Computation* 68(226): 559–583.

Brenner SC, Scott LR (1994) *The mathematical theory of finite element methods*. New York: Springer.

Chaumont-Frelet T and Nicaise S (2018) High-frequency behaviour of corner singularities in Helmholtz problems. *ESAIM: Mathematical Modelling and Numerical Analysis* 52(5): 1803–1845.

Christodoulou E, Elliotis M, Xenophontos C, Georgiou G (2012a) Analysis of the singular function boundary integral method for a biharmonic problem with one boundary singularity. *Numerical Methods for Partial Differential Equations* 28(3): 749–767.

Christodoulou E, Elliotis M, Xenophontos C, Georgiou G (2012b) The singular function boundary integral method for 3-D Laplacian problems, with a boundary straight-edge singularity. *Applied Mathematics and Computation* 219(3): 1073–1081.

Costabel M, Dauge M, Duduchava R (2003) Asymptotics without logarithmic terms for crack problems. *Communications in Partial Differential Equations* 28(5–6): 869–926.

Dauge M and Nicaise S (2017) Special issue: singularities, integral equations and electromagnetism preface. *Mathematical Method in the Applied Sciences* 40(2): 328–338.

Elliotis M, Christodoulou E, Georgiou G, Xenophontos C (2010) *the singular function boundary integral method for a 3-D Laplacian problem with an edge singularity*. Recent Development in Boundary Element Methods (a volume to honour John T Katsikadelis). WIT Press.

Elliotis M, Georgiou G, Xenophontos C (2002) The solution of Laplacian problems over L-shaped domains with a singular function boundary integral method. *Communications in Numerical Methods in Engineering* 18(3): 213–222.

Elliotis M, Georgiou G, Xenophontos C (2005a) Solution of the planar Newtonian stick-slip problem with a singular function boundary integral method. *International Journal for Numerical Methods in Fluids* 48(9): 1000–1021.

Elliotis M, Georgiou G, Xenophontos C (2005b) Solving Laplacian problems with boundary singularities: a comparison of a singular function boundary integral method with the p/hp version of the finite element method. *Applied Mathematics and Computation* 169(1): 485–499.

Elliotis M, Georgiou G, Xenophontos C (2006) The singular function boundary integral method for a two-dimensional fracture problem. *Engineering Analysis with Boundary Elements* 30(2): 100–106.

Elliotis M, Georgiou G, Xenophontos C (2007) The singular function boundary integral method for biharmonic problems with crack singularities. *Engineering Analysis with Boundary Elements* 31(3): 209–215.

Elliotis M, Charmpis D, Georgiou G (2014) The singular function boundary integral method for an elastic plane stress wedge beam problem with a point boundary singularity. *Applied Mathematics and Computation* 248(Dec): 93–100.

Elliotis M (2016) The singular function boundary integral method for the 2-D and 3-D Laplace equation problems in mechanics, with a boundary singularity. *Pure and Applied Mathematics Journal* 5(6): 192–204.

Elliotis M (2019) A mathematical model for a steady-state seepage flow of groundwater under a reinforced concrete dam. *Applied Computing and Geosciences* 1(Oct): 100003.

Fung YC (1977) *Foundations of solid mechanics*. New Jersey: Prentice-Hall Inc.

Georgiou GC, Olson L, Smyrlis G (1996) A singular function boundary integral method for the Laplace equation. *Communications in Numerical Methods in Engineering* 12: 127–134.

Karageorghis A (1992) Modified methods of fundamental solutions for harmonic and biharmonic problems with boundary singularities. *Numerical Methods for Partial Differential Equations* 8(1): 1–19.

Katsikadelis J (1991) Large deflections of plates on elastic foundation by the boundary element method. *International Journal of Solids Structures* 27(15): 1867–1878.

Li ZC (1998) *Combined methods for elliptic equations with singularities, interfaces and infinities*. Boston: Kluer Academic Publications.

Li ZC, Lu TT, Huang HT, Cheng A (2007) Trefftz collocation and other boundary methods – A comparison. *Numerical Methods for Partial Differential Equations* 23(1): 93–144.

Li ZC, Lu TT, Hu HY, Cheng A (2008) *Trefftz collocation methods*. Southampton, Boston: WIT Press.

Omer N, Yosibash Z (2019) Extracting stochastic stress intensity factors using generalized polynomial chaos. *Engineering Fracture Mechanics* 206(Feb): 375–391.

Schapira Y, Yosibash Z (2020) Asymptotic solution of the elasticity equations in the vicinity of an elliptical crack front. *Engineering Fracture Mechanics* 223(Jan): 106774.

Seshaiyer P, Suri M (1998) Conforming results for non-conforming hp methods: the mortar finite element method. *Contemporary Mathematics* 218: 453–459.

Stephan E, Whiteman JR (1988) Singularities of the Laplacian at corners and edges of three-dimensional domains and their treatment with finite element methods. *Mathematical Methods in the Applied Sciences* 10(3): 339–350.

Szabo BA, Yosibash Z (1996) Numerical analysis of singularities in two dimensions Part 2: Computation of generalized flux/stress intensity factors. *International Journal for Numerical Methods in Engineering* 39(3): 409–434.

Woo G, Kim S (2018) Stress intensity factors and finite element solutions for corner singularities. *East Asian mathematical journal* 34(5): 623–632.

Xenophontos C, Elliotis M, Georgiou G (2006) The singular function boundary integral method for elliptic problems with singularities. *SIAM J. Sci. Comput*. 28: 517–532.

Yosibash Z, Mittelman B (2016) A 3-D failure initiation criterion from a sharp V-notch edge in elastic brittle structures. *European Journal of Mechanics - A/Solids* 60(Nov-Dec): 70–94.

Yosibash Z, Schapira Y (2021) Edge stress intensity functions along elliptic and part-elliptic 3-D cracks. *Engineering Fracture Mechanics* 245(Mar): 107477.